19EB Fuel Coolant Interactions

19EB.1 Introduction

Fuel coolant interactions were addressed in the early assessment for the ABWR response to a severe accident. Subsection 19E.2.3.1 examined the hydrodynamic limitations for steam explosions and concluded that there was no potential for a large scale steam explosion. The pressurization of the containment from non-explosive steam generation was calculated in the analyses for the accident scenarios. The following subsections examine the available experimental database for its relevance to the ABWR configuration, and provide a simple, scoping calculation to estimate the ability of the ABWR containment to withstand a large, energetic fuel coolant interaction.

Challenges of the containment during a severe accident may result from fuel coolant interactions. Both the impulse and static loads are considered here. Fuel Coolant Interactions (FCI) may occur either at the time of vessel failure when corium and water fall from the lower plenum of the vessel, or when the lower drywell flooder opens after vessel failure has occurred.

The critical time constants for a steam explosion are considered in 19E.2.3.1. This analysis concludes that the critical rates for heat transfer and energy dispersal preclude a large scale steam explosion which could damage the containment. Nonetheless, this study was performed to examine the potential impact of a large steam explosion on the ABWR.

Several experiments which have provided insights to steam explosions are examined, and features of the ABWR are compared to previous plants to indicate the relative resistance of the ABWR to steam explosions. A scoping calculation is also performed to estimate the size of steam explosion the ABWR could withstand.

Four potential failure modes are considered. The transmission of a shock wave through water to the structure may damage the pedestal. Similarly, a shock wave through the airspace can cause an impulse load. However, since the gas is compressible, the shock wave transmitted through the gas will be much smaller than that which can be transmitted through the water. Therefore, this mechanism is not considered here. Third, loading is caused by slugs of water propelled into containment structures as a result of explosive steam generation. Finally, the rapid steam generation may lead to overpressurization of the drywell.

19EB.1.1 Probability of a Pre-flooded Lower Drywell

The configuration of the ABWR containment, shown in Figure 19EB-6, limits the potential for water to be in the lower drywell at the time of vessel failure. The vessel skirt is solid and there are no active injection systems in the lower drywell. Therefore, the only possible sources of water to the containment are the wetwell/drywell connecting vents, the passive flooder and the vessel itself.

The wetwell/drywell connecting vents connect the upper and lower drywell regions to the suppression pool. The connecting vent is a vertical channel which has a horizontal branch leading to the lower drywell. Therefore, in order for water flow from the upper drywell to enter the lower drywell, it would have to fall almost nine meters down the connecting vents, then turn to enter the lower drywell. This is not viewed to be a credible scenario.

For the water level in the wetwell to rise sufficiently to overflow into the connecting vents, approximately 7.2E5 kg (1.6E6 lbm) would have to be added to the containment. If the EPGs are followed, this would occur only if injection was being provided from an external source in the event that flow from the suppression pool was not available. This implies that the only available injection sources are the Firewater and RCIC Systems. The RCIC System may be the only system available in events initiated by station blackout. Examination of the cases in 19E.2.2.3 (SBRC sequences) and 19E.2.2.8 (NSRC sequences) indicates that enough water can be added by the RCIC System to lead to overflow from the suppression pool to the lower drywell. If the station blackout continues and the Firewater Addition System is not used to prevent core damage, vessel failure into a pre-flooded cavity can occur in these sequences. The results of the Level 2 analysis, depicted in Figure 19D.5-3 indicate that SBRC sequences with failure of the vessel (no IV) are an extremely small percentage of all core damage sequences. The Class IV ATWS sequences were treated very conservatively in the containment event trees. All of these sequences were presumed to lead to core damage with high releases. However, as indicated by the analysis in Subsection 19E.2.2.8, Class IV sequences do not necessarily lead to core damage. Several hours are available for the operator to take appropriate actions to terminate the event. A conservative factor is applied to Class IV events to estimate the frequency of sequences with core damage and a pre-flooded lower drywell. These sequences are an extremely small percentage of all core damage sequences.

The passive flooder is designed to open when the temperature in the lower drywell airspace reaches 533 K (500°F). This temperature is slightly less than the temperature of the steam in the vessel under normal operating conditions. However, any potential break flow would cool by flashing as it reaches the lower drywell. Therefore, the passive flooder will not open until after vessel failure.

A LOCA in the bottom head of the vessel is also a source of water which could be present in the lower drywell at the time of vessel failure. All of the penetrations in the lower head are small, and any loss of coolant accident through them is classified as a small break LOCA. A conservative estimate of the core damage frequency for events initiated by LOCAs in the bottom head is the frequency of all small break LOCAs which lead to core damage for the ABWR. Examining Table 19D.4-1, the fraction of all core damage events initiated by a small LOCA is extremely small.

The potential for a fuel coolant interaction which could threaten the containment may be bounded by summing the frequencies of the sequences with water in the lower drywell at the time of vessel failure. Three sequences were identified above. The total frequency of these

sequences is an extremely small percentage of all core damage sequences. Because this value is very small, it is judged that fuel coolant interactions will not have a significant impact on risk.

19EB.2 Applicability of Experiments

A large number of experiments have been performed to better understand FCI. Most of these experiments have been performed at bench scale with simulant materials. Freon-Water and Liquid Nitrogen/Water Systems are often used. While these experiments are necessary to understand the underlying physics of FCI, they are not directly applicable to the reactor condition. However, there are also several experiments performed with metal and oxides which provide insight to the potential for energetic FCI in a severe accident.

Other experiments, performed for different reasons, also yield some insights to FCI. Some experiments performed for debris coolability and core concrete interaction studies added water to the debris. With one notable exception, these experiments did not result in an energetic FCI. Finally, one experiment was performed to examine the impact of a water solid reactor cavity on direct containment heating. In the following subsection each of these experiments is examined for the insights into FCI and applicability to the ABWR.

19EB.2.1 Fuel Coolant Interaction Tests

A wide variety of experiments have been performed to investigate steam explosions. This subsection discusses results from selected experiments. Most of the experiments are prototypic of the reactor condition wherein debris falls into a pre-existing pool of water. The implications of these experiments on the potential for large, energetic FCI in the ABWR are also discussed.

Investigations into energetic fuel coolant interactions and steam explosions date back to 1950. Early experiments, including those by Long (References 19EB-1 and 19EB-2) and Higgins (Reference 19EB-3), identified the requirements for considerable mixing of the molten debris and water. Higgins and Lemmon (Reference 19EB-4) noted that the debris must be superheated and that the violence of the explosion increased with the melt temperature. Unfortunately, the triggers used in many of these experiments were very large. Thus, information about the propagation and energetics of these experiments is not applicable to reactor conditions.

One of the important parameters in determining the potential challenge to the containment from a steam explosion is the duration of the pressure pulse. Buxton and Benedick (Reference 19EB-5) performed a large series of experiments using iron-alumina thermite. The pressure traces for these experiments indicate an explosive pressure pulse of about 5 milliseconds.

The final, intermediate scale test performed at Sandia (Reference 19EB-6) used a corium thermite mass to simulate the materials which might be typical of a severe accident. As in the Buxton and Benedick experiment, the duration of the pressure pulse in these experiments was about 5 milliseconds. Three shakedown tests were performed using iron-alumina thermite with water in a crucible. In all of the tests spontaneous, self-triggered explosions occurred. In

contrast, all four of the corium tests were externally triggered which resulted in one run with a "weak explosion" and one with a "mild explosion". Two hypotheses were proposed to explain these results:

(1) The non-condensable gasses generated by oxidation stabilized the film boiling blanket, making it less susceptible to triggering;

(2) The UO_2 and ZrO_2 superheat was only about 300 K. It is possible that the debris froze before the trigger was initiated. This would prevent fine fragmentation of the debris.

Both these hypotheses have important implications for application to the severe accidents. Presuming a BWRSAR-type melt progression, the early pour of debris from the vessel would be metallic. In this case stabilization of the gas film around the debris could prevent a large mass of molten material from participating in a steam explosion. On the other hand, the superheat associated with a large oxidic melt is typically less than a few hundred degrees. Therefore, it is likely that the surface of the debris droplets would freeze. This would slow the heat transfer to the coolant and a steam explosion would not occur.

19EB.2.2 Experiments With a Stratified System

In some of the recent experiments performed to examine core concrete interaction, water has been added to the debris. As discussed in Subsection 19EB.1.1, the probability of a large amount of water in the lower drywell at the time of vessel failure is very small. After core debris is introduced to the lower drywell, it is flooded either by active systems or the Passive Lower Drywell Flooding System. Therefore, this is the most probable initial configuration for an FCI event in the ABWR.

Far fewer experiments have been performed in this stratified geometry than in the configuration of debris poured into water. Work by Bang and Corradini (Reference 19EB-7) used triggered Freon/Water and Liquid Nitrogen/Water Systems. In these studies the interaction zone for the vapor explosion is less than 1 cm thick. Assuming this depth is representative of reactor material, this would lead to the conclusion that less 3% of the ABWR core inventory could participate in an FCI event.

Prototypic materials have been used in a few core-concrete interaction experiments in which water is added to molten debris. The MACE and WETCOR tests added water to a pre-existing pool of debris. These tests involved fairly large masses of molten simulant to which water was added. Thus, the initial condition is a stratified pool in which water lies over the core debris. The materials and masses of the experiments are summarized in Table 19EB-1. No energetic fuel coolant interactions were observed to occur in the stratified configuration. The experiments typically indicated an early heat transfer phase in which the heat fluxes were on the order of 1.5 to 2 MW/m^2. Later, presumably after the formation of a crust above the molten debris pool, the

heat fluxes decreased. These heat fluxes are considered in Subsection 19EB.6.2 in bounding the non-explosive steam generation rates.

19EB.2.3 BETA V6.1

Recently, an energetic FCI occurred in the BETA facility. Experiment V6.1 was intended to represent the Bibilus reactors. These reactors have an annular pool of water around the pedestal cavity. BETA V6.1 was designed to determine the impact of these water pools on corium concrete interaction. The configuration of V6.1 is shown in Figure 19EB-1. The system consisted of a concrete crucible with an annular water pool which was vented back to the inner crucible via a small path. Molten iron alumina thermite was introduced into the cavity which was then allowed to ablate.

The debris eroded the concrete in the approximate shape shown in Figure 19EB-1. The superheat of the melt was very high since there was no water on the debris. Eventually, the sideward erosion caused the debris to reach the annular water pool at one local point. Instants later an explosion occurred. The bottom of the crucible was sheared off. There was severe damage to the facility. All of the instrumentation was destroyed and the melt injector was thrown several meters up, damaging the ceiling.

The energy required to do the damage has not yet been determined. However, the structure surrounding the test facility was fairly weak, unprotected sheet metal. Although the doors were blown open they were not damaged. Therefore, it is believed that the pressure spike may not have been very large.

The symmetry of the damage to the crucible indicates that the explosion was very symmetric. There was very little irregularity in the shearing of the bottom of the crucible. Thus, it is difficult to believe that the explosion began on one side of the crucible and propagated sideward. An alternate hypothesis has been proposed (Reference 19EB-8). When the debris penetrated to the annular pool, the steam generation rate increased. Since the annular compartment vents back to the center of the crucible via a small line, the pressure increased and water was forced back into the debris. The debris was still highly superheated at this time. The confinement of the system allowed for intermixing of the debris and water and prevented the pressure from being relieved. Thus, the damage caused to the system was not a result of a shock wave, but rather due to simple pressurization of a confined region.

The steam explosion observed in the BETA facility is not applicable to the ABWR system. Although suppression pool and vent system of the ABWR is located in an annulus around the lower drywell, there is adequate vent area to relieve the pressure in the wetwell drywell connecting vents. In fact, the BETA configuration is also much more restrictive than the Bibilus reactor it was intended to represent. This restrictive condition resulted in ingression of water into the melt. Since the ABWR configuration has much more vent area, water ingression will not occur.

Additionally, there was no water on top of the debris before penetration into the annulus. Thus, the molten debris in V6.1 was highly superheated. This is contrasted to the situation in the ABWR. The ability to use active systems, such as the Firewater Addition System, and the presence of the passive lower drywell flooder virtually ensure that there will be water above the debris in the ABWR. The area of the ABWR lower drywell is also very large which enhances coolability. The uncertainty analysis of Attachment 19EC indicates there is a low probability that significant core concrete attack will occur. Therefore, the initial contact mode observed in V6.1 is unlikely.

Even if CCI occurs and the pedestal is eroded to the wetwell drywell connecting vents. The presence of water above the debris will cause a crust to form. The temperature on the lower surface of the crust will be at the melt point of the debris. Within any molten region, the debris temperature will be nearly equal to the melt temperature due to convection in the debris pool. Thus, the addition of any water to the molten pool will cause the debris to freeze and a steam explosion will not occur.

The conditions which led to the explosion at the BETA facility are not prototypic of the ABWR. Due to operation of the flooder there is a small likelihood that the debris will ablate the side wall and enter the wetwell drywell connecting vents. This is examined in Attachment 19EC. Even if the debris does penetrate the pedestal to the connecting vents, the vent area in the ABWR is sufficient to relieve the steam generation caused by the initial contact of water and debris. Thus, water would not be forced into the melt as occurred at BETA. Finally, the superheat of the melt at the BETA facility was very high, whereas the superheat of any debris which contacted water in the ABWR would be low. Thus, debris would be easily solidified, reducing the heat transfer to the water and preventing rapid steam generation. Thus, the explosion in V6.1 does not indicate that containment damage will occur in the ABWR as a result of FCI.

19EB.2.4 High-pressure Melt Ejection Experiments

Sandia performed a series of experiments to examine the influence of water pools on the behavior of high-pressure melts in a Zion-like cavity (Reference 19EB-9). Two configurations were examined. In the SPIT-15 test debris was injected into a closed acrylic box. This allowed for visualization of the phenomena. In the SPIT-17 and HIPS experiments a Zion-like cavity was constructed. The basic configuration of the SPIT-17 and HIPS experiments is shown in Figure 19EB-2. The SPIT-17 cavity was made of aluminum while the HIPS experiments used reinforced concrete cavities.

In all of the experiments water was present in the cavity at the time of melt ejection. The inertia of the water prevented venting of the cavity. Thus, the steam generation in the cavity forced the region to pressurize and the structures were destroyed before gas flow from the end of the structure could relieve the pressure in the cavity.

It is interesting to compare these experiments to BETA V6.1. In both instances it appears that large pressure spikes were created when the debris and water were tightly confined. This early

confinement keeps the water and debris in close contact, and seems to lead to the fragmentation of the hot molten material which is a necessary precondition for steam explosions.

The results of this experiment are not applicable to the ABWR configuration. The lower drywell is not initially full of water and there is ample venting of the region. The extreme damage observed in these experiments appear to be consistent with that in BETA V6.1, both in the mode and magnitude of the damage to the facilities.

19EB.3 Explosive Steam Generation

This subsection presents a bounding analysis of the maximum steam generation rate which can occur for a given mass of corium interacting with water.

19EB.3.1 Phenomenology

Corium interactions with water can result in rapid steam generation. The rate of steam generation can be limited by the amount of corium or water present. Maximum generation for a given amount of corium occurs when enough water is present to completely quench the corium. Corium mass, surface area, temperature and heat transfer coefficient dictate the maximum rate when ample water is available.

Two configurations are possible for quenching in the ABWR. First, corium can exit the vessel when the lower drywell contains significant amounts of water. Corium exit from the vessel can be either by a slow pour (small vessel breach) or by a sudden drop (catastrophic failure of lower vessel head). Second, corium can enter a dry lower drywell and form a pool. Subsequently, the lower drywell is flooded with water and the debris is quenched. This situation, commonly referred to as a stratified geometry steam explosion, is the expected configuration for any large FCI in the ABWR.

Molten core debris is expected to be discharged from the vessel close to its liquidus temperature, 2600 K. Therefore, the maximum temperature in either the pour or stratified geometries will be 2600 K. The actual temperature will be lower due to heat loss by the debris prior to interaction with water. In the pour case, corium will transfer heat to the air surrounding the vessel as it falls. Any residual water in the lower drywell, as well as concrete beneath and air above the debris pool will absorb heat in the stratified geometry.

For rapid steam generation to occur in either situation, the ejected corium must break up into small particles. The analysis presented in Subsection 19E.2.3.1.4 demonstrated that corium breakup in the ABWR will be driven by Taylor instabilities. The smallest particles formed will be approximately 2.5 mm based on the Taylor critical wavelength. Debris breakup in the stratified geometry will also be governed by Taylor instabilities.

Crust formation will hinder debris breakup. Since corium is expected to exit the vessel near its liquidus temperature, any heat loss should contribute to crust formation. Furthermore, the outer debris surface will freeze rapidly after encountering water. Freezing will hinder further droplet

division because more energy will be required to fracture the outer crust than it does to overcome the liquid surface tension. This, in part, explains why self-triggering can be observed with some highly superheated metals, but is much less likely with molten core debris.

19EB.3.2 Bounding Analysis

Moody, et al., (Reference 19EB-10) determined the maximum steam generation rate during FCI based on a simplified thermal-hydraulic methodology. The steam formation rate from a single corium droplet assuming heat transfer to saturated water is:

$$\dot{m}_{g,\,d} = \frac{HA_d(T_{ci} - T_\infty)}{h_{fg}} e^{-t/\tau_h} \qquad \text{(19EB-1)}$$

where:

$\dot{m}_{g,\,d}$ = steam formation rate,

H = heat transfer coefficient,

A_d = surface area of a corium droplet,

T_{ci} = droplet surface temperature,

T_∞ = saturation temperature of water at the ambient pressure,

h_{fg} = latent heat of vaporization for water,

t = time from beginning of interaction,

τ_h = thermal response time.

Heat transfer from the droplet to the surrounding is dominated by convection and radiation. The heat transfer coefficient is:

$$\begin{aligned} H &= H_c + H_r \\ &= H_c + \frac{\sigma(T_{ci}^4 - T_\infty^4)}{(T_{ci} - T_\infty)}\varepsilon \end{aligned} \qquad \text{(19EB-2)}$$

where:

H_c = convective heat transfer coefficient,

H_r = radiative heat transfer coefficient,

σ = Stefan-Boltzmann constant,

ε = emissivity of the droplet.

Due to the high temperature of corium, convective heat transfer from the surface of the particle will be in film boiling regime. The maximum convective heat transfer coefficient that can be expected is that of enhanced film boiling, which is 390 W/m^2K. The emissivity suggested for use in MAAP (Reference 19EB-11) for corium is 0.85. This value will be used for this analysis.

If a mass of corium, M_c, interacts with water and breaks up into droplets of average radius, r, the number of droplets, N, will be given by:

$$N\left(\frac{4}{3}\pi r^3\right) = \frac{M_c}{\rho_c} \tag{19EB-3}$$

where:

ρ_c = density of corium.

The total steam generation rate of N corium droplets is:

$$\dot{m}_g = N\dot{m}_{g,d} = \dot{m}_{g,Max}e^{-t/\tau_h} \tag{19EB-4}$$

where the maximum generation rate is:

$$\dot{m}_{g,Max} = \frac{3M_cH(T_{ci} - T_\infty)}{\rho_c h_{fg} r} \tag{19EB-5}$$

This is the maximum steam generation rate that can occur for a given amount of corium broken up into small droplets in a large body of saturated water.

19EB.4 Impulse Loads

Rapid steam generation can produce a shock wave which imparts impulse loads to containment structures. Energetic FCIs, however unlikely, may occur in the lower drywell of the ABWR. Water in the lower drywell, which must be present for rapid steam generation, can transmit shock waves from the site of FCI to the walls of the pedestal. Shock waves which pass into the gas space above the water will be rapidly damped due to gas compressibility and will not represent any threat to containment integrity. If the impulse load is large enough, the pedestal will fail causing the vessel to tip. Tipping of the vessel would most likely lead to tearing of the

containment penetrations. The scoping analysis presented in this subsection estimates the amount of corium which can participate in a FCI without exceeding the impulse load capability of the pedestal.

19EB.4.1 Maximum Impulse Pressure

Moody, et. al., (Reference 19EB-10) determined the maximum pressure increase at the site of an FCI based on the steam generation rate given in Equation 19EB-5. His analysis applied the Rayleigh bubble equation to a single steam bubble with an equivalent volume of the many bubbles formed during interaction with N corium droplets of radius, r. Because the volume varies as r^3, this results in overestimation of the rate of bubble expansion. The bubble expansion rate dictates the pressure rise. Therefore, this analysis bounds the pressure generated by the maximum steam generation during FCI.

The maximum pressure increase of a single submerged steam bubble above the ambient pressure during its formation at the generation rate given in Equation 19EB-5 is:

$$\Delta P_{Max} = 0.178\left[\rho_1 \frac{(R_g T_\infty \dot{m}_{g,\,Max})^2}{R_o^4}\right]^{1/3} \qquad \text{(19EB-6)}$$

where:

ρ_1 = density of saturated water at the ambient pressure,

R_g = gas constant for steam,

R_o = starting radius for steam bubble growth.

The starting radius for bubble growth can be estimated by a spherical volume equal to the corium volume plus the total volume of water it vaporizes which in equation form is:

$$\frac{4}{3}\pi R_o^3 = \frac{M_c}{\rho_c} + \frac{M_c c_c (T_{ci} - T_\infty)}{h_{fg}\rho_1} \qquad \text{(19EB-7)}$$

where:

ρ_c = density of corium,

c_c = specific heat of corium.

The maximum pressure predicted by Equation 19EB-6 is shown in Figure 19EB-3 for participating corium masses from 0 to 30,000 Kg. The required corium properties were taken

from Table 19E.2-17. The steam and water properties are saturated conditions at two atmospheres. Two atmospheres is a likely containment pressure at vessel failure for the ABWR.

The peak pressure during impulse loading of the ABWR pedestal resulting from fuel coolant interactions should be bounded by the pressure shown in Figure 19EB-3. The pressure predicted by Equation 19EB-6 is conservative because of the assumptions which went into its creation. Furthermore, this is the pressure at the site of FCI. The pressure experienced by the pedestal wall will be reduced because the shock wave has to pass through some amount of water before it impinges on the wall. The pressure will decay as r^{-2} as it moves away from the source (Reference 19EB-12).

19EB.4.1.1 Impact of FMCRD Platform Grating (on FCI)

The FMCRD platform grating is located in the lower drywell at the elevation of the access tunnel. This rotating platform is circular and mounted on the rotating rail under the reactor vessel. There is an opening area at the center of the platform which is provided with a traveling rail for the CRD handling device. Gratings will be installed on both sides of the rail for maintenance personnel. Typically, the grating consists of 2.54 cm (1-inch) by 0.95 cm (3/8-inch) metal slats mounted edge-wise to form a grid with a grid size on the order of 2.54 cm (1 inch) by 5.08 cm (2 inch).

The presence of the grating could provide some increased fragmentation of the debris as the leading edge of the debris enters a pre-existing water pool. This will tend to increase the voiding of the pool. Because the structure of the grating is very open, there will be no significant limitations on the venting of steam generated below the grating. Increased voiding in the water pool will reduce the impulse loading from an FCI. This in turn will decrease the potential for early containment failure from FCI.

The grating will be ablated as the debris passes through it, in the same manner as the ablation of the bottom head. Therefore, the grating will have no impact on the severe accident performance after the initial debris relocation. Any late debris relocation would be a slow drip-like relocation which would fall straight through the ablated region of the platform.

19EB.4.2 Impulse Duration

The main difference between energetic fuel coolant interactions (steam explosions) and non-energetic interactions is the time in which the energy stored in the corium is transferred to the coolant. Short transfer times, on the order of milliseconds, indicate explosive reactions. Longer times are indicative of non-energetic interactions. Several fuel coolant interaction experiments involving corium simulants were reviewed in Subsection 19EB.2.2. Pulse widths were observed to be of the order 5 milliseconds or less for FCI.

19EB.4.3 Pedestal Capability

Detailed calculations of the capability of the ABWR pedestal to withstand impulse loading have not been performed. However, a simple elastic-plastic calculation can provide a capability which can be used for scoping analysis. This estimate can be compared to the maximum pressure expected during a FCI for a given amount of participating corium and the impulse duration. The pedestal in Grand Gulf (MARK III containment) was analyzed in NUREG-1150 (Reference 19EB-13) with regards to its ability to withstand pressure spikes generated by steam explosions. Since the ABWR pedestal is expected to be at least as strong as that of a MARK III, the impulse capability of the Grand Gulf pedestal can also be used for comparison.

19EB.4.3.1 Elastic-Plastic Calculation

A failure limit estimate based on a simple elastic-plastic calculation has been performed by Corradini (Reference 19EB-12). The assumptions made in this analysis are:

(1) The pedestal wall is thin compared to its diameter,

(2) The pressure loading is uniform both spatially and temporally,

(3) Failure is based on a strain criteria of μ (failure strain/yield strain) equal to 10,

(4) The pedestal wall is considered to be free standing.

The resistance to deformation, R_m, of the pedestal is:

$$R_m = \frac{\sigma_y \Delta_w}{R_w} \qquad \text{(19EB-8)}$$

where:

σ_y = yield stress of the pedestal wall,

Δ_w = thickness of the pedestal wall,

R_w = radius of curvature of the wall.

The natural period of the pedestal, T, can be calculated from:

$$T = 2\pi \sqrt{\frac{\rho_w R_w^2}{E_w}} \qquad \text{(19EB-9)}$$

where:

ρ_w = wall density,

E_w = Young's Modulus of the pedestal.

Since the pedestal is a composite structure, the determination of each of these parameters can be quite complicated. A conservative estimate of the resistance to deformation and the natural period can be obtained by using the following parameters:

σ_y = 175 MPa (value for the A441 steel plates which define the boundaries of the pedestal),

Δ_w = 6 cm (total thickness of the two A441 steel plates which define the boundaries of the pedestal, ignores steel webs and concrete fill),

R_w = 6.15 m (average radius of the pedestal),

ρ_w = 2,400 kg/m^3 (density of concrete fill between steel plates),

E_w = 200 GPa (typical value of steel).

Using these parameters yields: R_m = 1.7 MPa and T = 4.2 milliseconds.

The maximum response of elastic-plastic one-degree systems (undamped) due to rectangular load pulses is shown in Figure 19EB-4. The ratio of pulse duration, t_d, to natural period is the horizontal axis. The strain criteria, μ, forms the vertical axis. The relationship between these two axis parameters is given by a series of curves defined by the ratio of resistance to deformation, R_m, to the average pressure of an impulse, F_1. The amplitude of the square pulse can be conservatively estimated by the maximum pressure rise expected during a FCI, ΔP_{Max}, which is calculated in Subsection 19EB.4.1.

As discussed previously, the impulse duration of a FCI is expected to be approximately 5 milliseconds (Subsection 19EB.2.1). The ratio of t_d/T for this duration is 1.2. Using this ratio and a strain criteria of 10 yields a R_m/F_1 of approximately 1.0. This implies that the pedestal can withstand a ΔP_{Max} of 1.7 MPa.

The maximum ratio of R_m/F_1 in Figure 19EB-4 is 2.0. Using this ratio, the lower limit of the pedestal capability is estimated to be 0.85 MPa. The uncertainty in pulse duration (assumed to be 5 milliseconds) is irrelevant for the maximum ratio of R_m/F_1 because it is obtained for pulse durations much greater than the natural period of the pedestal.

This simple elastic-plastic calculation predicts that the pedestal can withstand a maximum pressure during a fuel coolant interaction of 1.7 MPa and that the conservative lower limit of the pedestal capability is 0.85 MPa. The amount of corium which must participate in a FCI to achieve this lower limit can be obtained from the analysis presented in Subsection 19EB.4.1

and summarized in Figure 19EB-3. The amount is 22,400 kg. The ABWR contains 235,000 kg of corium. Therefore, the ABWR pedestal can withstand a FCI involving 9.5% of the corium inventory.

19EB.4.3.2 Comparison to NUREG-1150 Grand Gulf Pedestal

The ability of the Grand Gulf pedestal to withstand steam explosions was considered in NUREG-1150 (Reference 19EB-13). The smallest impulse load expected to fail the pedestal was reported to be 0.024 MPa•s. This limit can be used for comparison to the ABWR because the ABWR pedestal is expected to be sturdier than that of a MARK III. For a pulse duration of 5 milliseconds, this impulse corresponds to a square wave pressure of 4.8 MPa. This value is significantly higher than the pressure predicted by the elastic-plastic scoping analysis. Alternatively, the lower pressure limit predicted by the elastic-plastic analysis (0.85 MPa) can be applied for 28 milliseconds before an impulse load of 0.024 MPa•s is exceeded. Both of these comparisons imply that the elastic-plastic analysis bounds the impulse load required to fail the pedestal.

19EB.4.4 Capability of the ABWR to Withstand Pressure Impulse

The ABWR pedestal has been shown in this scoping analysis to be capable of withstanding a peak pressure of at least 0.85 MPa during a steam explosion. The amount of corium required to produce this pressure impulse during a fuel coolant interaction was shown to be 22,400 kg. This represents 9.5% of the ABWR corium inventory. This is more than three times the maximum amount of debris which could participate in an FCI event based on the observations discussed in Subsection 19EB.2.2. Therefore, the ABWR pedestal is very resistant to the impulse loading which could occur in a severe accident. This failure mechanism need not be considered further in the containment event trees or the uncertainty analysis.

19EB.5 Water Missiles

Submerged steam formation resulting from fuel coolant interactions can be rapid enough to propel an overlying liquid mass. Impact loads can be imparted to containment structures if the liquid mass (water missile) is ejected from the water pool with a great enough velocity. Although a prediction of impact by a water missile does not imply damage, additional analysis would be needed to assess the structural response. The maximum height to which a water missile can rise will be determined in this subsection for a given amount of participating corium. The rise height will be compared to the distance between the expected water surface of a pre-flooded lower drywell and the bottom of the reactor vessel to determine if damage to the containment could occur. No other structures are considered because damage to them will not lead to containment failure.

19EB.5.1 Maximum Rise Height

Moody, et. al., (Reference 19EB-10) used the steam generation rate determined in Subsection 19EB.3.2 to predict the upward propulsion velocity and elevation characteristic of

a water missile. The maximum velocity that a water missile can obtain is the maximum radial expansion rate of the steam bubble formed during FCI. This expansion rate is:

$$\dot{R}_{\infty} = \frac{3}{5}\left[\frac{5}{2}\frac{R_g T_{\infty}\dot{m}_{g,\,Max}}{4\pi\rho_l R_{\infty}^2}\right]^{1/3} \qquad \text{(19EB-10)}$$

where:

R_{∞} = equilibrium steam bubble radius.

R_{∞} is equal to:

$$R_{\infty} = \left[\frac{3}{4\pi}\frac{M_c c_c (T_{ci} - T_{\infty})}{h_{fg}\rho_g}\right]^{1/3} \qquad \text{(19EB-11)}$$

where:

ρ_g = vapor density.

Balancing the kinetic and potential energies of a water missile yields:

$$\Delta y_{Max} = \frac{\dot{R}_{\infty}^2}{2g} \qquad \text{(19EB-12)}$$

where:

Δy_{Max} = maximum rise height a missile will rise above the water surface,

g = acceleration of gravity.

Maximum missile rise heights are presented in Figure 19EB-5 for participating corium masses of 0 to 30,000 kg.

19EB.5.2 Available Rise Height

The water level in the lower drywell will not be greater than suppression pool water level during a severe accident. The normal water level of the suppression pool is 6.10 meters below the bottom of the reactor vessel. Consequently, a water missile can rise approximately six meters before encountering any structure the damage of which could lead to containment failure.

19EB.5.3 Capability of ABWR to Withstand Water Missiles

The amount of corium which can participate in a FCI in the ABWR and not generate a pressure impulse which is expected to fail the containment is 22.4 Mg. This amount of corium will produce a water missile which will rise 1.75 meters (Figure 19EB-5). This rise height is significantly lower than the available rise height of 6 meters. Therefore, the pedestal will fail from impulse loading before the required amount of corium participates to elevate a water missile even to the bottom of the reactor vessel. For this reason, water missiles are not expected to play a role in determining if the ABWR containment fails due to fuel coolant interactions.

19EB.6 Containment Overpressurization

The final element of this study focuses on the pressurization of the containment which may occur during periods of rapid steam generation which may occur when corium is being quenched. In the highly unlikely event of an ABWR core melt which leads to vessel failure, the corium will fall into the lower drywell. There are ten connecting vents which join the lower drywell, the upper drywell and the wetwell, as shown in Figure 19EB-6. The pressure suppression containment prevents large increases in containment pressure by sparging the steam through the connecting vents to the suppression pool which condenses the steam. However, if the pressure rise is extremely rapid, the vents may not be able to clear before the containment is damaged. At even higher steam generation rates, the area from the lower drywell to the upper drywell could be too small and a pressure difference between the drywell regions could occur, failing the lower drywell. This analysis determines the steam generation rates for different limits on FCI. The maximum rate is then compared to the containment pressure capability to assess the potential for containment damage as a result of overpressure during an FCI event.

19EB.6.1 Methodology

This calculation compares the pressurization due to rapid quenching of corium to the pressure capability of the containment. Two non-explosive steam generation limits are considered. If there is a sufficiently large water mass, then the quenching of corium will provide the steam generation limit. If the mass of water limits the steam spike then the steam generation will be less than, or equal to, the water flow into the lower drywell. The impulse pressure limited mass, calculated in Subsection 19EB.3.1, is also considered.

If there is no water in the lower drywell at the time of vessel failure, then the maximum rate of steam generation at some later point in time is the rate at which water is introduced into the lower drywell. If there is still water in the lower plenum at the time of vessel failure, as predicted by MAAP-ABWR, then this source of water could react with the corium in the lower drywell. Water addition could also occur via the passive flooder, the use of the Firewater Addition System or by means of ECCS recovery. Each of these possibilities will be examined to determine the maximum rate at which water could be added to the lower drywell.

For most of the core melt sequences in the ABWR PRA there will not be water in the lower drywell at the time of vessel failure (Subsection 19EB.1.1). Nonetheless, an evaluation will be performed assuming that corium falls into a pre-existing pool of water and is quenched instantaneously. This will provide a limit on the peak containment pressure which could result from quenching of debris as it falls into the lower drywell. For the ABWR, the majority of sequences with vessel failure occur at low pressure. Therefore, gravity is the driving force for the flow of corium from the lower head of the vessel to the lower drywell. Both MELCOR and MAAP predict that the vessel fails at the penetrations for low pressure melts. After the initial hole is formed, the hole ablates due to the flow of hot corium. In order to determine the sensitivity of the ABWR containment to rapid steam generation 40% of the total UO_2 mass is assumed to be molten at the time of vessel failure. This value is consistent with the upper limit for molten debris used in the uncertainty analyses for direct containment heating (Subsection 19EA.2.1.4).

Two potential limits for pressurization due to steam generation are considered. First, the pressurization of the lower drywell is determined considering the limit of the vent area from the lower drywell to the upper drywell. This determines any limits for the assumption that the upper and lower drywell regions have good communication and will respond similarly to the pressurization. Second, the response of the Pressure Suppression System is evaluated. Drywell pressurization rates are used to determine the vent clearing response which is in turn used to determine the peak containment pressure as a function of the pressurization rate.

19EB.6.2 Maximum Steam Generation Rates

The first step in determining the peak pressures that may result from fuel coolant interactions is to determine the maximum steam generation rates. The steam generation can be limited either by the available water or the available corium. Both of these possibilities will be considered separately.

19EB.6.2.1 Water Added to Debris

There are four potential sources of water addition to the lower drywell. First, in a MAAP-type core melt progression, there may be water in the lower plenum at the time of vessel failure. After the corium falls into the lower drywell, the water will follow through the ablated hole in the lower plenum. Second, the lower drywell passive flooder opens when its fusible material melts. Water from the wetwell is then driven by gravity into the lower drywell. Third, the Firewater System may be used to add water to either the vessel or the upper drywell. In either case, water will eventually flow into the lower drywell at the firewater injection rate. Finally, if the ECCS is recovered, these systems could be used to inject water into the vessel which again will flow into the lower drywell.

19EB.6.2.1.1 Water Inventory from Lower Plenum

If there is water in the lower plenum at the time of vessel failure, then it will fall into the lower drywell after the corium. Under these conditions, the flow will be driven by gravity through the

ablated vessel failure. The expected failure mode for a BWR is penetration failure (Reference 19EB-14). A parametric study was performed to determine the final, ablated area resulting from different numbers of CRD penetrations. The study was conducted by varying the number of vessel penetrations presumed to open at the time of vessel failure. Since this affects the initial area of the vessel failure, multiple penetration failures have higher initial debris pour rates. As seen in Figure 19EB-8, the final area varied from 0.06 m^2 for 10 penetrations failed to 0.08 m^2 for one penetration. The final area is smaller for cases with multiple penetration openings because the duration of the debris pour is shorter. In order to bound the flow of water into the lower plenum, a value of 0.1 m^2 is used which results in a maximum mass flow rate of 1020 kg/s.

19EB.6.2.1.2 Passive Flooder Flow

The passive flooder is composed of ten pipes connecting the lower drywell to the suppression pool with fusible material at the lower drywell end which opens when it reaches a specified temperature. This is shown schematically in Figure 19EB-7.

The flow from the wetwell into the lower drywell is driven by the difference in the water height, h, between the connecting vents and the flooder. The flow rate is given by:

$$\dot{m} = \rho A \sqrt{2gh} \qquad \text{(19EB-13)}$$

where:

$\dot{m}$ = water mass flow into the lower drywell (kg/s),

ρ = density of water (kg/m^3),

A = total area of passive flooders (m^3),

g = acceleration of gravity (9.81 m/s^2),

h = driving head of water (m).

The maximum flow through the passive flooder would occur when the pressure difference between the wetwell and the drywell was sufficient to open the vacuum breakers, and the suppression pool is cold. Assuming a suppression pool temperature of 303.2 K (30°C), ρ = 996 kg/m^3. The total area of the passive flooders is A = 0.081 m^2. Assuming that the pool is at the high water level and the pressure difference between the wetwell and drywell is at the full open setpoint of the vacuum breakers, the height of water above the passive flooder is h = 4.75, which yields a maximum flow rate of $\dot{m}$ = 780 kg/s. The flow rate will typically be less than this maximum because the drywell pressure is greater than wetwell and the first row of vents will be clear.

19EB.6.2.1.3 ECCS and Firewater Flow

The ECCS and Firewater System are both capable of adding water to the vessel which would flow into the lower drywell. The Firewater System has a direct-drive diesel pump which does not rely on AC power, so it is available even during a station blackout event. The ECCS is dependent on AC power; and, thus, will not be available during station blackout but could inject water during recovery late in a severe accident. The ECCS System has a flow rate far greater than the Firewater System. Therefore, no determination of the firewater flow is necessary. The maximum ECCS flow will be bounded by the runout flow of the ECCS pumps. The actual flow will be somewhat smaller due to the flow losses at higher velocities when all of the pumps are operating simultaneously.

There are two HPCF Systems, each with a runout flow of 230 kg/s (3800 gpm), and three LPFL Systems with flow of 265 kg/s (4200 gpm). The RCIC System is not considered since the vessel will be depressurized. The total water addition rate to the lower drywell is 1250 kg/s.

19EB.6.2.2 Steam Generation Rate for Pre-flooded Lower Drywell

For the ABWR, it is very unlikely that there is water in the lower drywell at the time of vessel failure. Thus, steam generation is usually limited by the availability of water. However, there may be sequences for which there is ample water, and the limitation on the steam generation rate is the energy of the quenching corium. Thus, it is prudent to determine the maximum steam generation from this limit if there were a large water supply available. A large mass of water is assumed to be present in the lower drywell for this portion of the analysis.

A wide number of analyses have been performed to determine the mode of vessel failure. While there are still some uncertainties in the details of the analysis, the work performed to date provides overwhelming indication that a BWR vessel fails at the penetrations (References 19EB-15 and 19EB-16). Once there is some flow through a penetration, the molten material will begin to ablate the hole. Neglecting the change in the driving force for the flow of molten material, the maximum flow rate will occur when the hole size is maximized as the mass is exhausted.

In some MELCOR-type analyses, the corium quenches in the lower plenum of the vessel. It subsequently heats up and causes vessel failure. Therefore, there is little corium molten at the time of vessel failure. The flow rate of corium from the vessel is limited by the rate at which the corium melts in the vessel. Conversely, using a MAAP-type analysis, the corium does not quench in the lower plenum. Thus, there is a large molten mass at the time of vessel failure. Since this will result in larger flow rates than the MELCOR-type model, the MAAP results will be used to determine the corium flow rate for this analysis.

MAAP-ABWR (as well as MELCOR) uses the Pilch model for the ablation of the penetration (Reference 19EB-11). The velocity of the corium through the vessel failure is approximately constant; therefore, the ablation rate of the failure is linear. A series of MAAP-ABWR runs were performed which examined the flow rate of molten debris and vessel failure area as a

function of the number of failed penetrations. The results of these calculations are shown in Figures 19EB-8 and 19EB-9. The maximum rate of debris ejection from the vessel is about 6000 kg/s. Assuming this material quenches as it is ejected, the steam generation rate is about 2800 kg/s.

The experimental heat flux observed when molten core debris simulants are poured into water is on the order of 1.5 to 2.0 MW/m^2 based on the floor area. Using the upper bound on the experimental observations, the maximum steam generation rate for the ABWR is 80 kg/s. This is far below the value determined above for the instantaneous quenching of debris for a bounding debris pour rate.

19EB.6.2.3 Explosive Steam Generation Rates

Based on the examination of the impulse loading calculation of Subsection 19EB.4.3.1, the ABWR can withstand the shock wave which corresponds to 22.4E3 kg of core debris. The maximum steam generation rate associated with this amount of debris is 4100 kg/s (Subsection 19EB.3.2).

19EB.6.2.4 Maximum Steam Generation

The maximum steam generation rates for each of the mechanisms described above are summarized in Table 19EB-2. Based on these results, the limiting scenario is the maximum steam explosion from the scoping study. Therefore, even though this event is far larger than the expected steam generation rate, the containment pressurization will be estimated using this value.

19EB.6.3 Containment Pressurization

The containment peak pressures may be calculated based on the flow rates determined above. The results given below are for the most restrictive pressurization rate. Three limits are considered. The first condition is the flow rate of steam from the lower drywell to the upper drywell. Second, the time period before the suppression pool vents open must be considered. Finally, the quasi-steady condition of flow from the drywell to the wetwell through the suppression pool is considered.

19EB.6.3.1 Drywell Connecting Vent Flow

Consideration of the flow through the drywell/wetwell connecting vents is important to ensure that there is adequate vent area to allow the upper and lower drywells to communicate freely. If the flow is restricted a significant pressure difference could exist between the upper and lower drywell regions. This could potentially result in lower drywell region failure. Using the maximum steam generation rate and an effective area of about 11.25 m^2 in the drywell/wetwell connecting vents, the pressure difference between the upper and lower drywell regions is less than 0.15 MPa.

19EB.6.3.2 Vent Clearing

If the drywell pressure is higher than the wetwell pressure at the time of the FCI, then steam flow to the wetwell can begin immediately. However, if the vents are not open, the pressure must accelerate the water in the vents to allow steam flow. During this interval the pressure in the drywell will rise quickly.

Assuming that the initial drywell and wetwell are at equal pressures maximizes the time for vent clearing. The time to vent clearing is calculated based on analysis by Moody (Reference 19EB-17). This model requires the pressurization rate for the drywell. The pressurization rate is determined by assuming a steam generation rate and using the ideal gas relationship for steam. The pressure rise in the drywell due to steam generation is then calculated using the pressurization rate and the time to vent clearing. Using the maximum steam flow rate, a pressure rise of 0.17 MPa is calculated.

19EB.6.3.3 Horizontal Vent Flow

After the vents have cleared, steam will begin to flow from the drywell to the suppression pool. The drywell pressure during this time is equal to the wetwell pressure plus the flow and water heads. Using conservative assumptions and the maximum steam flow rate, the drywell wetwell pressure difference is found to be 0.16 MPa.

19EB.6.4 Summary of Overpressurization Limits

Based on the calculations presented above, the maximum pressure rise in the lower drywell due to fuel coolant interactions occurs just before the wetwell/drywell connecting vents clear. At this time a pressure spike in the lower drywell of 0.17 MPa may occur. FCI events of the magnitude considered here occur when there is a large mass of unquenched debris which comes into sudden contact with water. In the ABWR this only occurs early in the course of a severe accident when the wetwell pressure is well below the COPS setpoint, typically at about 0.2 MPa. Even if the wetwell pressure were near the COPS setpoint of 0.72 MPa, the pressure difference between the drywell and wetwell would be equal to the design pressure of 0.27 MPa. There will be ample margin to the ultimate capability. Therefore, FCI leading to overpressurization failure of the lower drywell is not a credible event.

Concerning the upper drywell region, a conservative calculation based on the maximum steam generation rate given in Table 19EB-2 indicates that the maximum pressure in the upper drywell is the wetwell pressure plus 0.172 MPa. Again, considering that FCI events of the magnitude considered here occur when there is a large mass of unquenched debris which comes into sudden contact with water, the drywell will be well below even the service level C pressure of 0.72 MPa. Therefore, one would not expect upper drywell failure as a result of FCI.

The only FCI event one could hypothesize to occur late in the accident is the recovery of ECCS just before containment failure. However, in the ABWR design the passive flooder ensures that there is water above the debris. The addition of ECCS water will not cause increased heat

transfer from the molten debris. Therefore, FCI leading to containment failure late in a severe accident has been ruled out by design.

The rapid steam generation rates which can occur due to bounding fuel coolant interactions do not lead to failure of the containment structure or opening of the rupture disk in the ABWR. Therefore, no further consideration of steam generation rates is required.

19EB.7 References

19EB-1 G. Long, “Explosions of Aluminum and Water”, Aluminum Company of America, New Kensington, Pennsylvania, ALCOA Report 2-50-33, August 1950.

19EB-2 G. Long, “Explosions of Molten Aluminum and Water”, Metal Progress, Volume 71, p. 107, May 1957.

19EB-3 H.M. Higgins, “The Reaction of Molten Uranium and Zirconium Alloys with Water”, Aerojet Report 2914-2, Azusa, California, April 1955.

19EB-4 A.W. Lemmon, “Explosions of Molten Aluminum and Water”, Light Metals, 1980, (C. Minn, Ed.), Proceedings of Technical Sessions Sponsored by TMS Light Metals Committee at the 190th AIME Annual Meeting, p.817.

19EB-5 L.D. Buxton and W.B. Benedick, “Steam Explosion Efficiency Studies”, Sandia National Laboratory, SAND/79-1399, NUREG/CR-0947, November 1979.

19EB-6 L.D. Buxton, W.B. Benedick and M.L. Corradini, “Steam Explosion Efficiency Studies: Part II - Corium Experiments”, NUREG/CR-1746, SAND/80-1324, Sandia National Laboratory, October 1980.

19EB-7 K.H. Bang and M.L. Corradini, “Vapor Explosions in a Stratified Geometry”, Nuclear Science and Engineering, Volume 108, Number 1, May 1991.

19EB-8 M.L. Corradini, personal communication, June 24, 1992.

19EB-9 W.W. Tarbell, et. al., “Pressurized Melt Ejection into Water Pools”, NUREG/CR-3916, SAND84-1531, Sandia National Laboratories, March 1991.

19EB-10 F.J. Moody, R. Muralidharan, S.S. Dua, “Assessment of Ex-Vessel Steam Pressure Spikes in BWR MARK II Containments”, 17th Water Reactor Safety Information Meeting, NUREG/CP-0104, October 1989.

19EB-11 “MAAP 3.0 B Computer Code Manual”, EPRI NP-7071-CCML, Volume 2, November 1990.

19EB-12 M.L. Corradini, et. al., “Ex-Vessel Steam Explosions in the MARK II Containment”, NUREG-1079, Appendix C, December 1985.

19EB-13 "Severe Accident Risks: An Assessment for Five U.S. Nuclear Power Plants", NUREG–1150, Volume II, Appendix C, December 1990.

19EB-14 J. L. Rempe, "Light Water Reactor Lower Head Failure Analysis (Draft)", NUREG/CR-5642, Idaho National Engineering Laboratory, December 1990.

19EB-15 J. L. Rempe, "BWR Lower Head Failure Assessment for CSNI Comparison Exercise", EGG-EAST-9609, April 1991.

19EB-16 S. A. Hodge and L. J. Ott, "Failure Modes of the BWR Reactor Vessel Bottom Head", ORNL/M-1019, May 1989.

19EB-17 Frederick Moody, "Introduction to Unsteady Thermofluid Mechanics", John Wiley and Sons, 1990.

19EB-18 J. M. Biggs, "Introduction to Structural Dynamics", McGraw-Hill Inc., 1964, p. 72.

Table 19EB-1 Core Concrete Interaction Tests with Water Addition to Debris

Experiment	Simulant	Debris Mass (kg)	Water Addition
MACE M0	UO_2 - ZrO_2 - Zr	130	Flooded after attack started
MACE M1	UO_2 - ZrO_2 - Zr	400	Flooded after attack started, upper crust was not fully molten
MACE M1B	UO_2 - ZrO_2 - Zr	400	Flooded after attack started, no crust above debris
WETCOR	Al_2O_3 - CaO	34	Water added at 1 liter/s

Table 19EB-2 Maximum Steam Generation for Steam Spikes

Water Limited Cases	
Flow from lower plenum at the time of vessel failure	1020 kg/s
Passive flooder	780 kg/s
Recovered ECCS	1250 kg/s
Debris Limited Case	
Debris falling into cavity is quenched instantaneously	2800 kg/s
Experimentally observed limit for debris poured into water	80 kg/s
Explosive Steam Generation	
Scoping result for shock wave capability	4100 kg/s

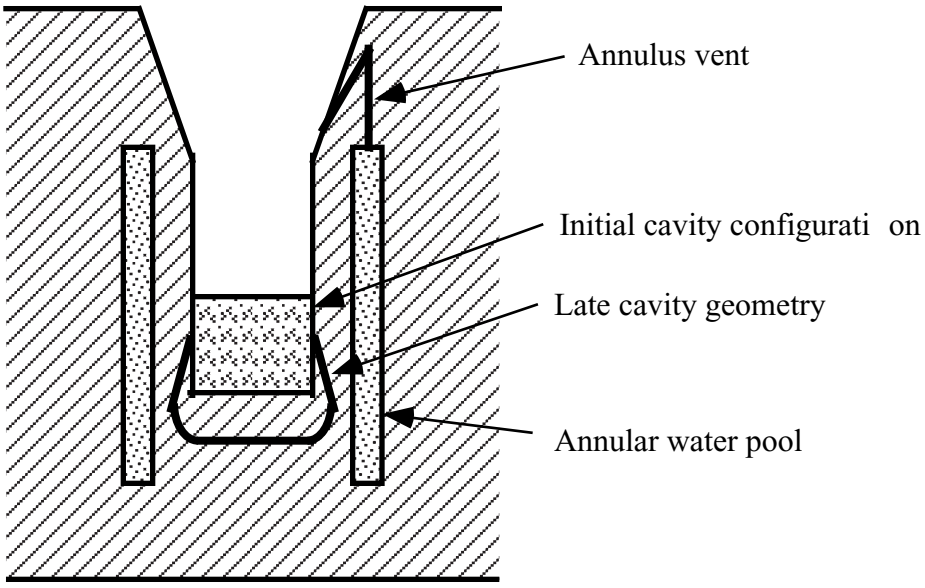

Figure 19EB-1 BETA V6.1 Configuration

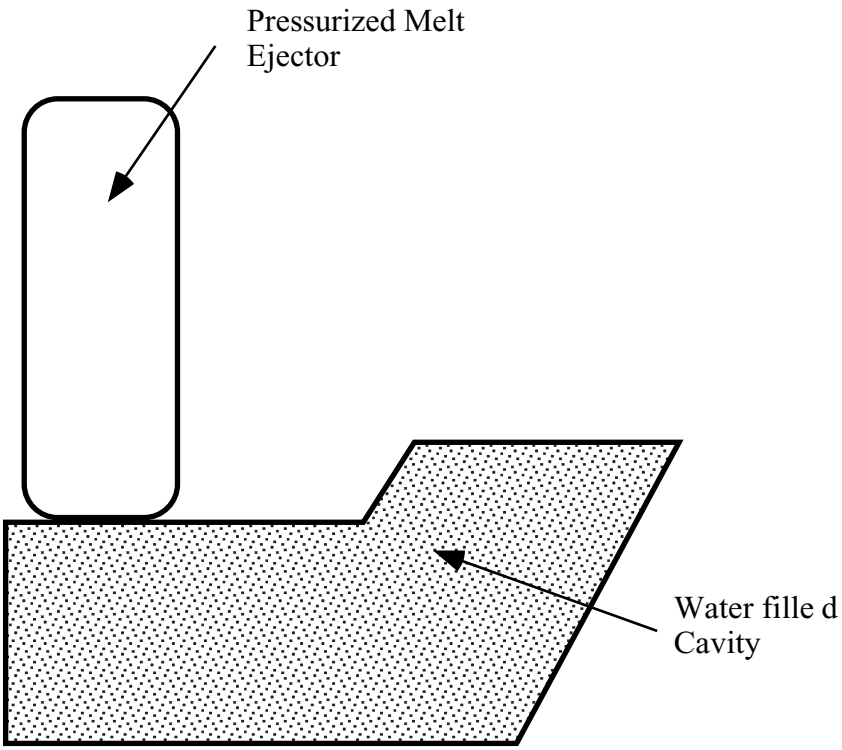

Figure 19EB-2 HIPS Experimental Configuration

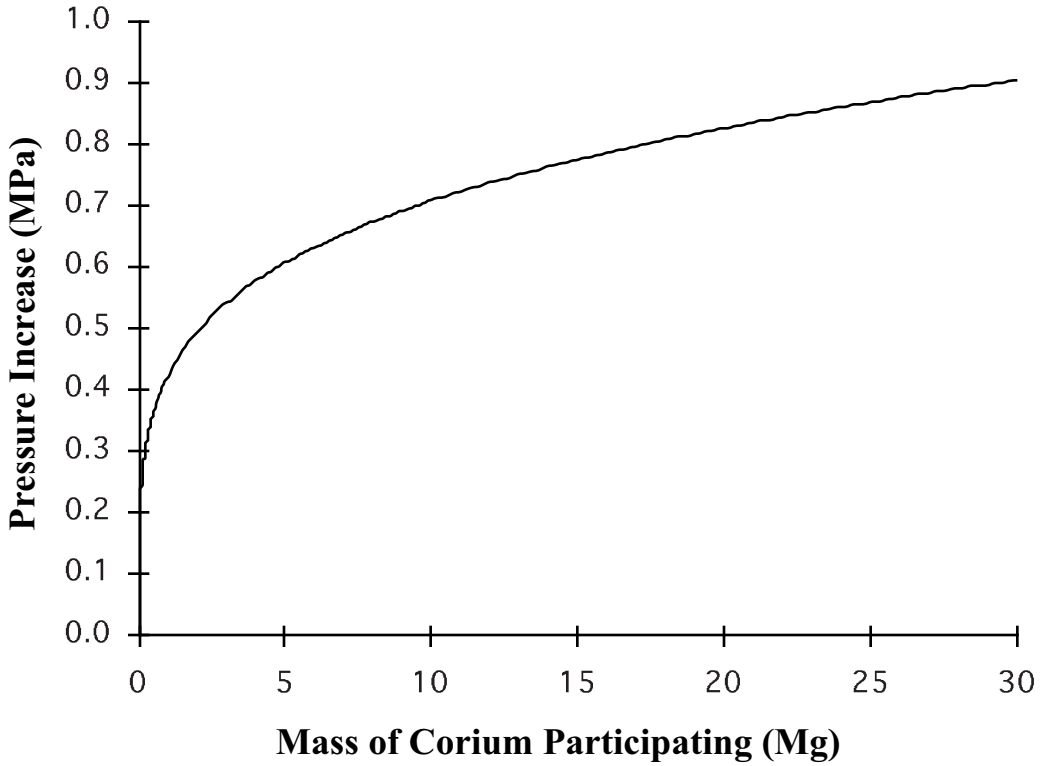

Figure 19EB-3 Peak Impulse Pressure from FCI

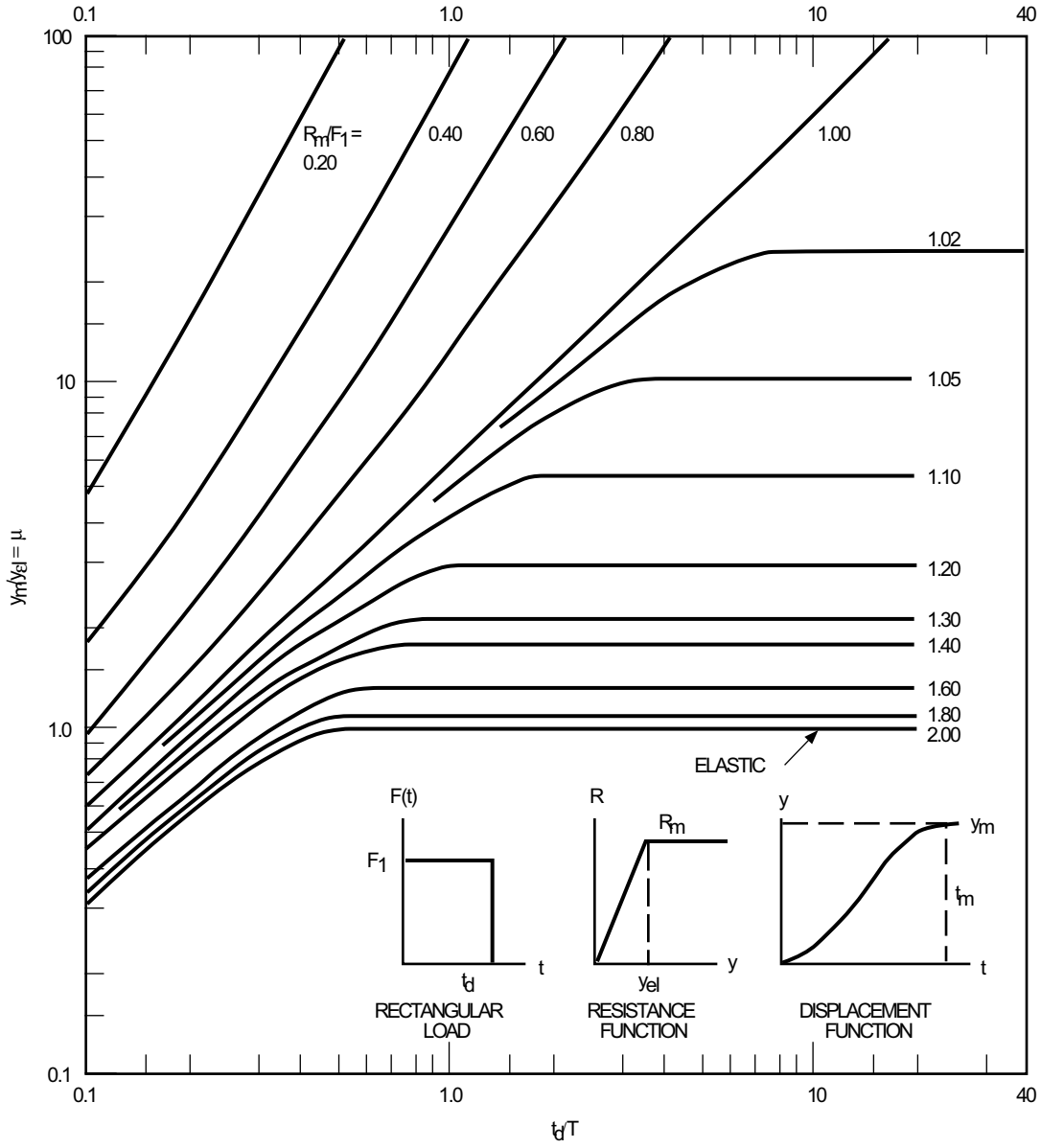

Figure 19EB-4 Maximum Response of Elastic-plastic One-degree Systems (Undamped) Due to Rectangular Load Pulses (Reference 19EB-18)

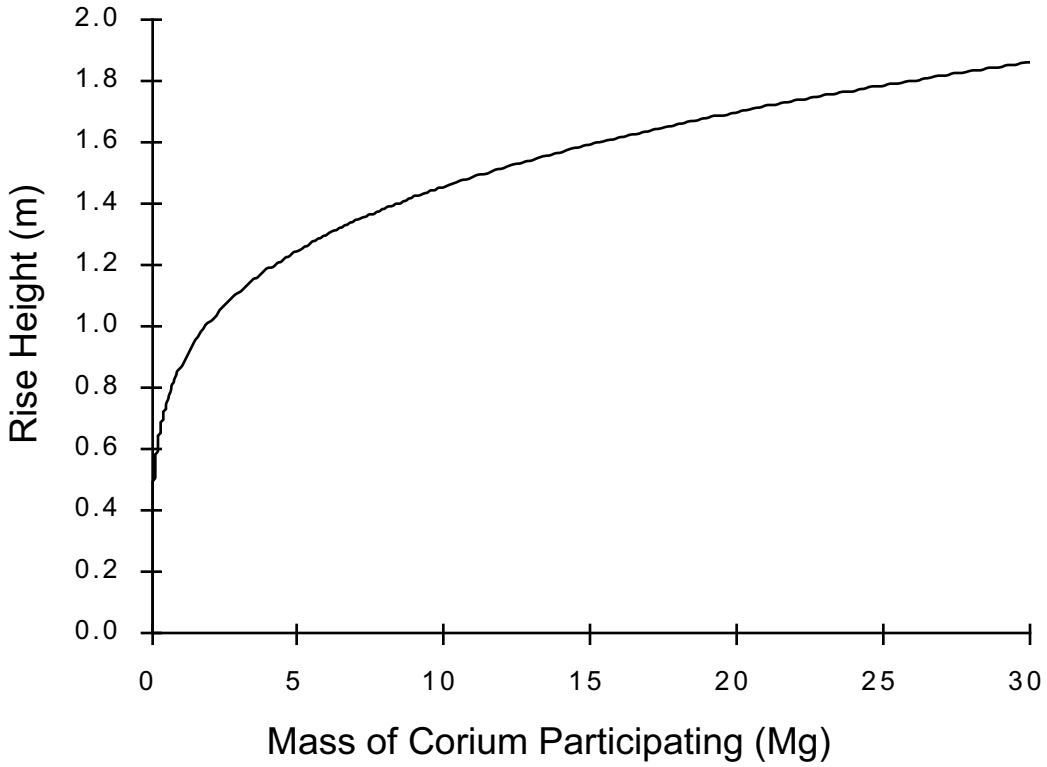

Figure 19EB-5 Rise Height of Water Missile

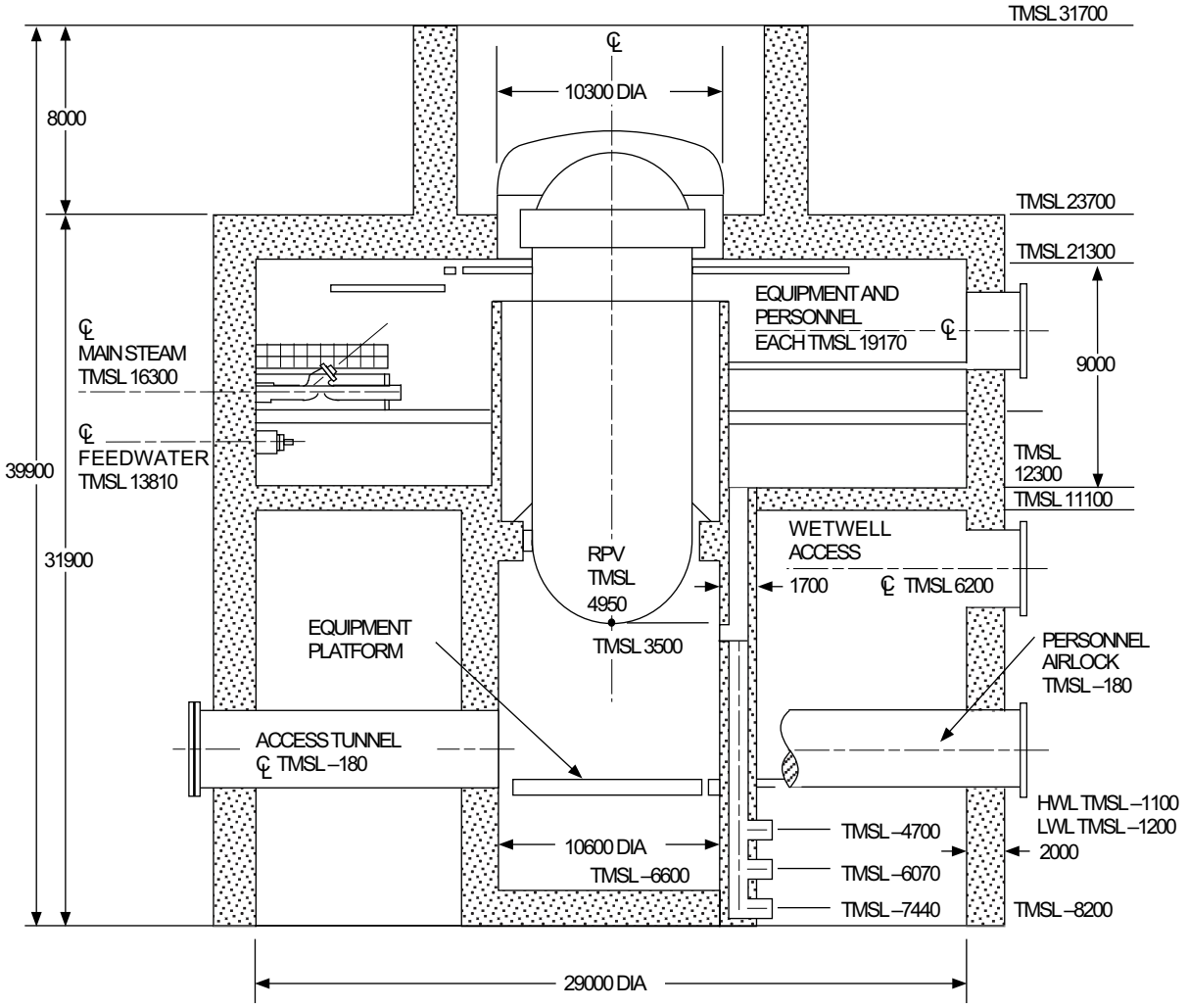

NOTES:
1. DIMENSIONS ARE IN MILLIMETERS

Figure 19EB-6 ABWR Containment Configuration

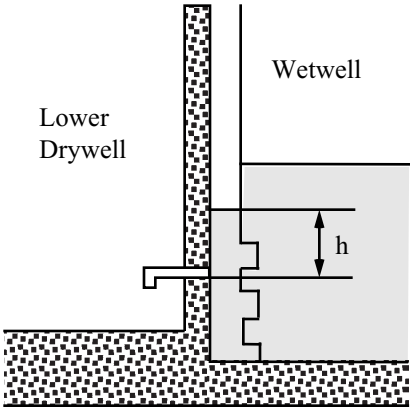

Figure 19EB-7 Pressure Head for Lower Drywell Flooder Flow

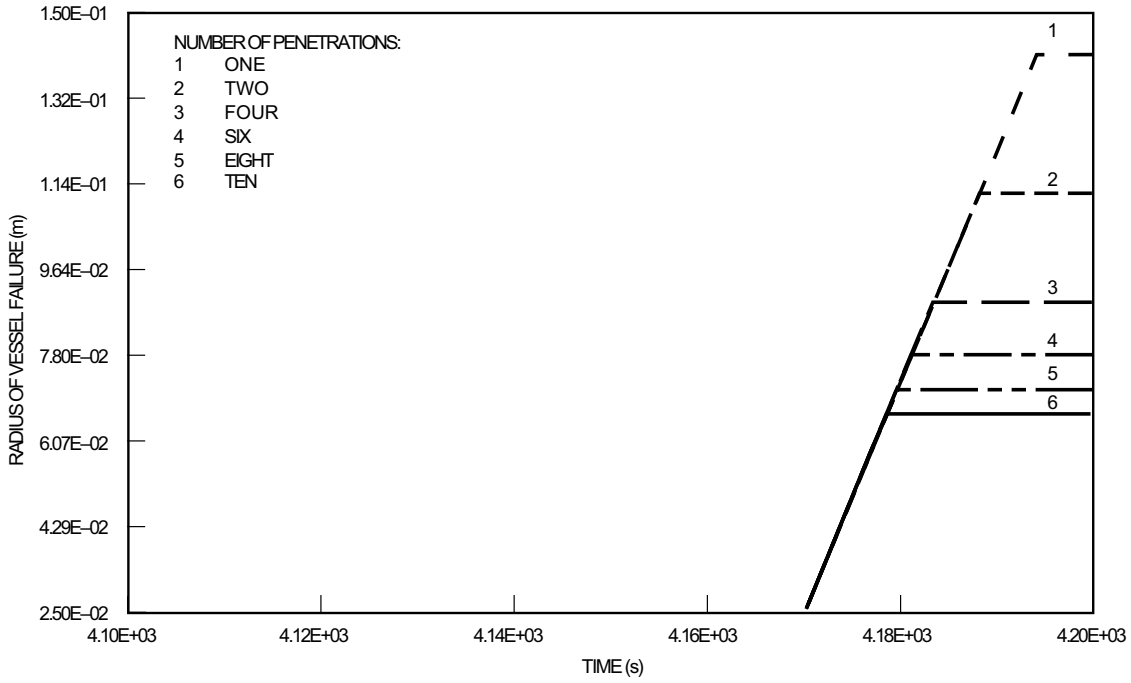

Figure 19EB-8 Ablated Radius of Vessel Failure

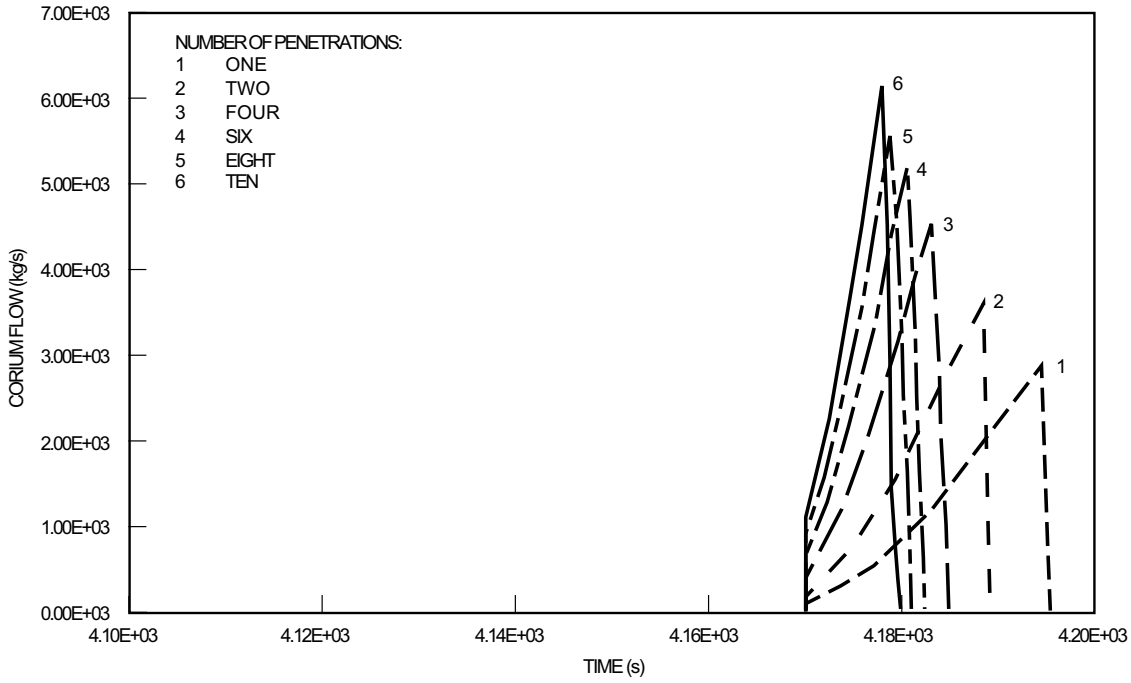

Figure 19EB-9 Mass Flow of Core Debris Through Vessel Failure